

Pinning force scaling analysis of Fe-based high- T_c superconductors

M. R. Koblishka

*Experimental Physics, Saarland University, Campus,
Building C 6 3, D-66123 Saarbrücken, Germany.*

M. Muralidhar

*Superconducting Materials Laboratory,
Department of Materials Science and Engineering,
Shibaura Institute of Technology, 3-7-5 Toyosu, Koto-ku, Tokyo 135-8548, Japan.*

(Dated: October 10, 2018)

Abstract

Pinning force data, F_p , of a variety of Fe-based high- T_c superconductors (11-, 111-, 122- and 1111-type) were analyzed by means of a scaling approach based on own experimental data and an extensive collection of literature data. The literature data were mostly replotted, but also converted from critical current measurements together with data for the irreversibility line when available from the same authors. Using the scaling approaches of Dew-Hughes [1] and Kramer [2], we determined the scaling behavior and the best fits to the theory. The data of most experiments analyzed show a good scaling behavior at high temperatures when plotting the normalized pinning force $F_p/F_{p,\max}$ versus the irreversibility field, H_{irr} . The resulting peak positions, h_0 , were found at ≈ 0.3 for the 11-type materials, at ≈ 0.48 for the 111-type materials, between 0.32 and 0.5 for the 1111-type materials and between 0.25 and 0.71 for the 122-type materials. Compared to the typical results of $\text{Bi}_2\text{Sr}_2\text{CaCu}_2\text{O}_{8+\delta}$ ($h_0 \approx 0.22$) and $\text{YBa}_2\text{Cu}_3\text{O}_{7-\delta}$ ($h_0 \approx 0.33$), most of the 122 and 1111 samples investigated show peak values higher than 0.4, which is similar to the data obtained on the light-rare earth 123-type HTSC like $\text{NdBa}_2\text{Cu}_3\text{O}_y$. This high peak position ensures a good performance of the materials in high applied magnetic fields and is, therefore, a very promising result concerning the possible applications of the Fe-based high- T_c superconductors.

[1] E. J. Kramer, J. Appl. Phys. **44**, 1360 (1973).

[2] D. Dew-Hughes, Philos. Mag. **30**, 293 (1974).

I. INTRODUCTION

The development of the iron-based pnictide¹ and selenide² high- T_c superconductors has stimulated a vast research effort on these materials, even though their transition temperatures are still not as high as the cuprate materials. From the viewpoint of possible applications, the superconducting transition temperatures of the pnictide materials are more similar to MgB_2 with a T_c of around 40 K, but the pnictides are also of ceramic nature and share many features with the cuprates like the extremely high values for the upper critical field, H_{c2} ^{3,4}. In the meantime, there are several Fe-based high- T_c superconductors known which can be classified into four main families (11-, 111-, 122- and 1111-type); the 122-family can also be made up from Fe-pnictides as well as from selenides. Most research on these materials is devoted to clarify the superconducting nature, offering a different approach as the cuprates. In this field, several reviews were already given in the literature^{3,5-7}.

Concerning possible applications of these materials, the grain boundary problem also plays an important issue for the Fe-based superconductors as discussed in Refs.^{8,9}. Due to this reason, the preparation of epitaxial thin films seem to be the most interesting direction. However, an important general property of a superconducting material is the flux pinning behavior, as flux pinning will rule the achievable critical current densities, the position of the irreversibility line and hence, effects of flux motion and creep. In order to perform such studies, homogeneous materials with a high content of the superconducting phase are required. This demand can be fulfilled with single crystals of the respective phase, but also with epitaxially grown thin films or phase-pure polycrystalline samples. Therefore, some research efforts had to be invested to obtain materials of such quality¹⁰⁻¹⁵.

The best tool to study details of the underlying flux pinning mechanism(s) is the scaling behavior of the flux pinning forces, $F_p = j_c \times B$, determined from the critical current densities, j_c . Such scaling was found to be useful already on the conventional superconductors in the works of Kramer¹⁶ and Dew-Hughes (DH)¹⁷. A scaling of F_p was obtained when plotting the normalized pinning force $F_p/F_{p,\text{max}}$ versus the reduced field $h = H_a/H_{c2}$, where H_{c2} denotes the upper critical field. This scaling implies $F_p = H_{c2}(T)^m \cdot f(h)^n$ with m and n being numerical parameters describing the actual pinning mechanism; $f(h)$ depends only on the reduced magnetic field, h . In the literature, several pinning functions $f(h)$ are described depending on the size and character of the defects providing the pinning based on the study

of conventional conventional, hard type-II superconductors^{18–21}. The scaled pinning force data were then fitted to the functional dependence given by

$$F_p/F_{p,\max} = A(h)^p(1-h)^q \quad (1)$$

with A being a numerical parameter, and p and q are describing the actual pinning mechanism. The position of the maximum in the F_p plot, h_0 , is given by $p/p+q$. In the model of DH, six different pinning functions $f(h)$ describing the core pinning using Eq. (1) are given. (1) $p=0$, $q=2$: normal, volume pinning; (2) $p=1$, $q=1$: $\Delta\kappa$ -pinning, volume pins; (3) $p=1/2$, $q=2$: normal, surface pins; (4) $p=3/2$, $q=1$: $\Delta\kappa$ -pinning, surface pins; (5) $p=1$, $q=2$: normal, point pins; and (6) $p=2$, $q=1$: $\Delta\kappa$ -pinning, point pins. Additionally, (3) is predicted by Kramer¹⁶ for shear-breaking in the case of a set of planar pins. The $\Delta\kappa$ -pinning is nowadays called δT_c -pinning²³. In a recent work²⁴, these six functions plus the ones for magnetic pinning were analyzed and it was found that they are linearly dependent, so some functions could be removed from the analysis. In the present case, we regard only the 6 functions mentioned above.

For various high- T_c cuprate materials, a reasonably good scaling of F_p is found as well, however, experiments have shown that the appropriate scaling field is the irreversibility field H_{irr} instead of H_{c2} . The use of the irreversibility field for the scaling was already discussed in Refs.^{25–27}; H_{irr} represents the upper limit of strong flux pinning, not H_{c2} as in the case of the conventional superconductors, as by definition $F_p \rightarrow 0$ at $H = H_{\text{irr}}$. In general, one can state that any determination of the parameters p and q from scaling laws is more significant than one obtained only from measurements of the irreversibility line.

Good pinning force scalings were reported in $\text{YBa}_2\text{Cu}_3\text{O}_{7-\delta}$ (Y-123), the light-rare-earth (LRE)-123 systems like $\text{NdBa}_2\text{Cu}_3\text{O}_{7-\delta}$ (Nd-123), $\text{GdBa}_2\text{Cu}_3\text{O}_{7-\delta}$ (Gd-123), $\text{SmBa}_2\text{Cu}_3\text{O}_{7-\delta}$ (Sm-123) and in the ternary LRE-compounds like $(\text{Nd}_{0.33}\text{Eu}_{0.33}\text{Gd}_{0.33})\text{Ba}_2\text{Cu}_3\text{O}_y$ (NEG) and $(\text{Sm}_{0.33}\text{Eu}_{0.33}\text{Gd}_{0.33})\text{Ba}_2\text{Cu}_3\text{O}_y$ (SEG)^{28–33}. The peak position of the scaling obtained ranges from 0.33 up to 0.5; the latter indicating the presence of the δT_c -pinning. The temperature range covered is mainly between 60 K and T_c , which is on one hand corresponding to the experimentally available magnetic field range, and on the other hand also containing the most interesting features like the fishtail peak. Furthermore, it was attempted in²⁷ to include the effects of flux creep in the DH model, but it turned out that especially the peak position h_0 is independent of creep effects. For more details, see the reviews given in

Refs.^{26,31,32}. The addition of nanoparticles to the superconducting matrix of the NEG system may lead to an apparent non-scaling behavior as shown in Ref.^{34,35}. In the case of Bi-based cuprate superconductors, the scaling leads to a peak position of $h_0 \approx 0.22$, which indicates the dominance of grain boundary pinning. In Bi-2223, a distinct non-scaling was observed indicating the change of the dominating pinning mechanism with temperature; the peak position shifts from 0.33 to 0.2 with increasing temperature³⁶. The other cuprate materials fit in this basic scheme depending on the degree of anisotropy, see the data in Refs.^{31,32,37}. Very recently, the pinning force scaling were reviewed by Sandu³⁸, also presenting the data of MgB_2 and with various additions to increase the flux pinning.

In the case of the iron-based superconductors, which consist of four main families, the pinning force scaling was obtained as well, also here mainly in the high temperature range which is accessible to the experiments. From the very beginning, one can see here a wider range of chemical dopings which causes a larger variation of the pinning force scaling as compared to the cuprate materials. Therefore, it is important to have a comparison of the available experimental data in order to discuss the flux pinning properties of these materials in detail.

In the present work, the present literature data of the flux pinning scaling are collected together and compared to each other. A total of 31 Fe-based superconducting compositions was retrieved from the literature^{39–65}. However, in order to achieve the goal of a valid comparison of the data, several data sets of the literature had to be replotted and reworked to enable such a comparison. Additionally, some own data are presented.

II. EXPERIMENTAL PROCEDURE AND ANALYSIS DETAILS

The flux pinning data are normally obtained via an elaboration of magnetic data measured by VSM- or SQUID magnetometry. Additionally, also data from electric transport measurements can be converted into flux pinning data. Here, it is important to note that the criteria for determining the critical current density and the irreversibility line must be the same for a given experiment. The reduced field, $h = H_a/H_{\text{irr}}$, is normally determined from the irreversibility fields according to a voltage criterion of $1 \mu\text{Vcm}^{-1}$ (i.e., the same criterion as applied for the j_c determination). In case of magnetization data, the criterion for determining H_{irr} is typically chosen as $1 \times 10^4 \text{ A/cm}^2$.

In several papers in the literature, the pinning force scaling is performed using the peak field of a fishtail peak, H_p , or the field where the maximum pinning force occurs, $H(F_{p,\max})$, instead of H_{irr} . H_p or $H(F_{p,\max})$ are experimentally directly accessible, so several authors prefer these fields, whereas the determination of H_{irr} requires the use of a criterion, which can be arbitrarily fixed. However, the scaling is not always properly done, so one has to carefully check the procedures applied. Therefore, one has to re-plot the according data sets in order to allow a direct comparison of the results. Some authors have only presented data for the peak position, h_0 , and not the full parameters of a corresponding fit. These data sets were fitted by taking the parameters from the respective master curve, and the fit was started using the basic parameters of the DH model. The results of these treatments are indicated in Tables 1-4 by using italics. In some cases, the pinning force data or critical current densities are published without showing the results for H_{irr} , so these data sets had to be excluded from the present analysis.

III. RESULTS AND DISCUSSION

In the following, the results of the pinning force scaling are presented for each of the four families of Fe-based superconductors. In Tables 1-4, all the contributions are sorted according to the publication year, and the type of sample (sc denotes single crystal, film, tape or polycrystalline) and some comments to the scaling are given. Figures 1-4 contain the determined pinning functions according to the parameters given in Tables 1-4. To enable an easier comparison of all the data, the data of the single crystals (sc) are plotted using filled symbols, the data of thin films and tape samples are plotted using open symbols. Data of different samples but of the same author are drawn using the same symbols and color, but with different lines.

A. 122-family

In the case of the 122-family (both pnictides and selenides), the largest number of works was performed concerning the pinning force analysis. The 122-family shows some importance for possible applications^{3,8,9}, so not only single crystals, but also epitaxial thin films and IBAD tapes were investigated in the literature. The peak positions determined range

between 0.22 and 0.5, with a remarkable exception of the data by L. Fang *et al.*⁴², which show peaks in the pinning force scaling as high as 0.68. In this work, also effects of irradiation on the flux pinning properties were investigated. The irradiated samples show indeed higher peak positions, which indicates the importance of flux pinning provided by a variation of the transition temperature, T_c .

Table 1 summarizes all pinning force scaling data published in the literature so far; the resulting pinning functions are plotted in Fig. 1 in order to enable a direct comparison of the data; the data set of the iron selenides (13) is indicated by a darker background in Table 1.

The available F_p -data show a clear tendency towards h_0 values higher than 0.33. However, it is important to note here that the peak positions larger than 0.33 can only be reached by an additional flux pinning contribution of the δT_c -type; the flux pinning provided by normal conducting particles and obstacles can only yield h_0 -values up to 0.33. Furthermore, it is remarkable that the data of thin films and IBA samples (7,10-13, marked using open symbols) show peak positions located at 0.22 to 0.33, which is also seen for films of other iron pnictide families. This indicates that the pinning landscape created by the substrate provides a strong pinning contribution, independent from the material properties.

The data of the single crystalline materials (1-6,8,9,13,15,17-19) are plotted in Fig. 1 using filled symbols. The data (7) and (10) exhibit a typical non-scaling over the entire temperature range – a good scaling is only obtained at higher temperatures close to T_c with a high h_0 , whereas at lower temperatures, the peak position is shifting towards smaller values. This behavior indicates a change of the dominant flux pinning mechanism with increasing temperature.

The data (3), (4) and (5) are single crystals with different doping, where each of the three crystals exhibits a distinct scaling behavior.

The data sets (2), (11), (15) and (19) are the ones with the highest peak position, h_0 ; while the data (12) show a peak at 0.33, but an extremely broad scaling curve, which yields strong flux pinning in the high-field regime. The data of the iron selenide (13) fit well to the other family members; the peak position, h_0 , is found at 0.32.

The data of the polycrystalline material (16) are not much different from the single crystal data of the same composition (6). The pinning function (6) was also observed in own SQUID-data of a single crystal, which are not shown here.

B. 1111-family

In the 1111-family, only some investigations of the flux pinning force scaling are reported; but also on various types of materials (single crystals, polycrystalline samples and films). All pinning force scaling data are collected in Table 2 and Figure 2. It is striking to see that the literature data do not follow any common behavior as all reported pinning force scalings yield a different peak position, h_0 . Interestingly enough, practically all data with the exception of the films (3) point to h_0 values larger than 0.33, which indicates a strong contribution of the δT_c -pinning in this type of material. Also here, the data measured on the IBAD tape exhibit the lowest peak position, which is, however, comparable to that of the 122-family data and coincides well with the Kramer theory. The data set (1) exhibits an extremely broad and high peak in the scaling diagram⁵⁵, even though the sample measured is of the polycrystalline type. The resulting h_0 is 0.57, which indicates a strong contribution of the δT_c -type.

The data (2) stem from the only single crystals measured in the literature⁵⁶. The authors have plotted their data in a scaling versus $H(F_{p,max})$, but for their analysis they correctly use an adapted version of the scaling law of the form $f(h) = h^p(2-h)^q$, which accounts that the maximal value of $H(F_{p,max})$ is 2 instead of 1 (their figure D3). For this reason, their determined values of q and p correspond well with the DH theory, and the peak position of the $F_p/F_{p,max}$ vs. $h = H_a/H_{irr}$ -plot can be calculated directly to $h_0 = 0.5$. For a cross check of the data, it was necessary to extract the H_{irr} -data from their paper. However, the data published stem from a transport measurement employing pulsed currents, whereas the F_p -data were obtained from a SQUID magnetometer. Luckily enough, $H_{irr}(T)$ can be extracted from their $F_p(H)$ -graphs (their figure D2). According to the authors, the possible pinning centers of the δT_c -type may originate in the local phase variation due to the oxygen or/and fluorine inhomogeneities.

The thin film data (3)⁵⁷ exhibit a peak position at 0.33, and the published data were shown to fit excellently to the Kramer theory, which is similar to the findings of other thin film materials.

The authors of (4)⁵⁸ had plotted their data again in a scaling versus $H(F_{p,max})$, but did not perform any fits to the theory. Here, the data could be reworked in the same way like that of Ref.⁵⁶, allowing them to be included here. Also here the peak position in the F_p -scaling

of 0.42 indicated flux pinning provided by δT_c -type pinning being active in the samples. The data (5) are exceptional in the sense that these authors⁶⁰ calculated F_p -data and showed in their paper a kind of scaling but only for one temperature (20 K), however, for various Y-doping concentrations. Nevertheless, a fit to these data provided a very high peak position of 0.71, which is the highest value measured so far. Also, these materials, although being polycrystalline, exhibit a very large irreversibility field which is just outside the experimental field range of 16 T. Besides the fluorine substitution at oxygen site, the substitution of Nd^{3+} with a relatively smaller ion like Y^{3+} creates lattice defects in $\text{NdFeAs}_{0.7}\text{F}_{0.3}$ and thereby improves the flux pinning capability of the system. Therefore, one may state here that it is obviously possible to even further increase the δT_c -type pinning contribution within the 1111-family, which already shows the highest peak positions of all Fe-based superconductors.

C. 11-family

The 11-type material may be an interesting one for applications as it does not contain a toxic material like As and no expensive rare-earth material, so the production costs could be lowered. Therefore, some investigations concerning the pinning force scaling on this type of material can be found in the literature. These data^{61–64} are summarized in Table 3 and Figure 3. Figure 3 shows clearly that the peak positions of the pinning force scaling are all located between 0.28 and 0.33, indicating a flux pinning being dominated by small normal-conducting particles. Therefore, one can say that the flux pinning in the 11-family behaves similar to pure YBCO material. Additionally, the pinning function of the data set (13) of the 122-family is drawn here for comparison as this material is also a iron selenide material. Even though the peak position of this data set is located at 0.32, the high-field side of the pinning function is different and more similar to the other 122-type data.

D. 111-family

In this type of material, only one report concerning the pinning force scaling is reported so far. The work of Shlyk *et al.*⁶⁵ reports a good scaling of F_p versus the peak field, $H(F_{p,\text{max}})$ in Ga-doped LiFeAs . They obtained $p = 2.06$ and $q = 0.71$ from a fit to the Kramer theory. However, as the peak position in the pinning force scaling diagram is calculated via

$h_0 = p/p + q$, this would yield $h_0 = 0.74$. This would be unreasonably high, so the data set had to be completely reworked. The irreversibility field, H_{irr} , could be determined from their Fig. 3 and the given functional dependence. Plotting then the data in the form $F_p/F_{p,\text{max}}$ vs. h yields $p = 3.73$ and $q = 3.98$ as shown in Table 4. The peak position determined here, h_0 , is still larger than 0.33, so the main conclusion of Shlyk *et al.* remains valid. This shows that the Ga-doping is introducing a stronger variation of T_c as compared to undoped samples of the same type. Additionally, the critical current densities of an undoped sample were measured in Ref.⁶⁵, but no F_p -scaling was given which would allow a comparison.

E. Remarks and analysis of the pinning force data

The present collection of pinning force data allows to draw some important conclusions about the flux pinning behavior in the Fe-based superconductors.

- (i) the data of practically all thin films and IBAD materials show only small values of $h_0 \approx 0.33$, which reflects the specific pinning landscape of the films on a substrate. These characteristic defects cause a flux pinning with $h_0 \approx 0.2$ to 0.33. The high density of substrate-induced defects yields a much stronger contribution to the flux pinning, and follows the Kramer theory of planar pins. In this sense, the mostly weaker δT_c -pinning contribution provided by the material disorder does not have an influence on the resulting flux pinning behavior.
- (ii) The 1111- and 122-families show a clear tendency towards the presence of a pinning contribution by a local variation of the transition temperature. Such a spatial variation of the superconducting gap parameter which corresponds to a spatial variation of the transition temperature, T_c , was accordingly observed in low-temperature STM data of $\text{Ba}(\text{Fe}_{0.9}\text{Co}_{0.1})_2\text{As}_2$ in the review⁶ and in Refs.^{66,67}.
- (iii) The strongest contribution of the δT_c -type pinning is observed in the 1111-family, where the replacement of Nd by Y leads to the formation of strong lattice defects providing a strong δT_c -pinning contribution. Furthermore, the variation of the peak position, h_0 , is extremely strong; there are not two data sets which yield approximately the same h_0 -values. This is a clear indication that more characterization experiments

are needed in this family. The observation of Ref.⁶⁰ indicates that one may find still more materials with a strong flux pinning.

- (iv) The 122-type family consists of iron pnictides and selenides, but the overall behavior of the flux pinning scaling is similar, with a tendency towards the δT_c -contribution, which is especially visible on the high-field side of the scaling graph.
- (v) The flux pinning data of the 11-family obtained in the literature are strikingly similar to each other, yielding peak positions between 0.27 and 0.32. These materials behave therefore very similar to pure Y-123 material, and the flux pinning is of the collective type.
- (vi) In the 111-family, there is currently only one report on flux pinning, but these data indicate that doping strongly increases the δT_c -type pinning contribution.

The flux pinning properties of the Fe-based superconductors show a large variety of behaviors as illustrated in Figs. 1 to 4 and Tables 1 to 4. This is also reflected in the variation of the scaling parameters p and q , which often deviate from the DH values of 1 and 2 for the normal point pinning and the δT_c -type point pinning. The values for p range between 0.23 and 3.73, the ones of q between 0.33 and 4.7. Values larger than 2 do not exist in the model of DH. However, here it is important to note that the relation between p and q , which is manifested by the peak position h_0 , is always in a reasonable range. In many cases, the fitting curves show deviations especially at the high-field side of the scaling diagram, which can be explained by flux creep effects. Such a behavior was already discussed in Ref.²⁷, and this may also lead to sets of p and q being different from the DH model.

The 122- and 1111-families exhibit a clear tendency towards a strong contribution of the δT_c -pinning, which is manifested by the peak positions of the scaling diagrams being larger than 0.4. The work of Ref.⁶⁰ demonstrated that by chemical doping this contribution can be strengthened, so their material exhibits the highest peak position measured so far in any type of high- T_c superconductor. Therefore, the chemical doping enables to tune the flux pinning behavior also in most of the iron pnictide and selenide compounds.

The data available in the literature for the 1111-family are largely scattered as not two reports yield the same peak position of the pinning force scaling. Therefore, it is difficult to give conclusions here, but the strong δT_c -pinning contribution is already evident. Further

work is needed here to fully understand the flux pinning behavior in these materials. The chemical doping of the superconducting compounds leads obviously to a strong spatial variation of the superconducting properties, which may create a situation similar to the ternary 123-type compounds^{30,33,68}. However, detailed measurements by, e.g., low-temperature STM and $m(T, B)$ magnetization field-cooling curves is still lacking in the literature.

From the 122-type iron selenides and the 111-family, there are still only one data set of each published in the literature. Recent reports like Ref.⁶⁹ show that different chemical compositions also yield different shapes of the magnetization loops, which also indicates that the flux pinning behavior of the 122-iron selenides will also exhibit a large variety.

Concerning possible applications of the iron-based superconducting materials, one can state that the flux pinning scaling behavior is in all cases strongly different from that of MgB_2 , which has a similar value of the transition temperature. Therefore, this will enable high-field applications of the iron-based superconducting materials, as their behavior is more similar to that of the cuprate high- T_c superconductors.

IV. CONCLUSIONS

In this contribution, the literature data of the flux pinning force scaling in iron pnictides and selenides are summarized. The data obtained by many authors could be included directly in the analysis, while some data sets scaled by the field of the pinning force maximum had to be reworked and replotted. Finally, the results of 30 different measurements are compared to each other. From this, some important conclusions concerning the further development of these materials towards possible applications can be drawn. The 122- and 1111-families exhibit a clear tendency towards a strong δT_c -pinning contribution to the flux pinning; the data of Y-doped $\text{NdFeAs}_{0.7}\text{F}_{0.3}$ exhibit the highest peak position of the pinning force scaling measured on any high- T_c superconducting material. In contrast to this, the 11-family shows a typical collective flux pinning. Of the 111-family, only one experiment exists in the literature, but also here the chemical doping seems to introduce the δT_c -pinning contribution.

ACKNOWLEDGMENTS

One of the authors (M.R.K) thanks D. Johrendt and E. Wiesenmayer (LMU München) for the polycrystalline 122-sample.

- ¹ Y. Kamihara, T. Watanabe, M. Hirano, and H. Hosono, *J. Am. Chem. Soc.* **11**, 3296 (2008).
- ² J. G. Guo, S. F. Jin, G. Wang, S. C. Wang, K. X. Zhu, T. T. Zhou, M. He, X. L. Chen, *Phys. Rev. B* **79**, 180520 (2010).
- ³ A. Gurevich, *Rep. Prog. Phys.* **74**, 124501 (2011).
- ⁴ C. Senatore, R. Flükiger, M. Cantoni, G. Wu, R. H. Liu, and X. H. Chen, *Phys. Rev. B* **78**, 054514 (2008).
- ⁵ Y. Kamihara, *Hyperfine Interact.* **208**, 123 (2012).
- ⁶ J. E. Hoffman, *Rep. Prog. Phys.* **74**, 124513 (2011).
- ⁷ M. R. Eskildsen, E. M. Forgan, and H. Kawano-Furukawa, *Rep. Prog. Phys.* **74**, 124504 (2011).
- ⁸ J. H. Durrell, C.-B. Eom, A. Gurevich, E. E. Hellstrom, C. Tarantini, A. Yamamoto and D. C. Larbalestier, *Rep. Prog. Phys.* **74**, 124511 (2011).
- ⁹ J. D. Weiss, C. Tarantini, J. Jiang, F. Kametani, A. A. Polyanskii, D. C. Larbalestier and E. E. Hellstrom, *Nature Mater.* **11**, 682 (2012).
- ¹⁰ K. Iida, J. Hänisch, M. Schulze, S. Aswartham, S. Wurmehl, B. Büchner, L. Schultz, and B. Holzapfel, *App. Phys. Lett.* **99**, 202503 (2011).
- ¹¹ S. R. Ghorbani, X. L. Wang, M. Shahbazi, S. X. Dou, K. Y. Choi, and C. T. Lin, *Appl. Phys. Lett.* **100**, 072603 (2012).
- ¹² C. J. van der Beek, G. Rizza, M. Konczykowski, P. Fertey, I. Monnet, Thierry Klein, R. Okazaki, M. Ishikado, H. Kito, A. Iyo, H. Eisaki, S. Shamoto, M. E. Tillman, S. L. Bud'ko, P. C. Canfield, T. Shibauchi, and Y. Matsuda, *Phys. Rev. B* **81**, 174517 (2010).
- ¹³ D. S. Inosov, T. Shapoval, V. Neu, U. Wolff, J. S. White, S. Haindl, J. T. Park, D. L. Sun, C. T. Lin, E. M. Forgan, M. S. Viazovska, J. H. Kim, M. Laver, K. Nenkov, O. Khvostikova, S. Kühnemann, and V. Hinkov, *Phys. Rev. B* **81**, 014513 (2010).
- ¹⁴ T. Ishibashi, Y. Nakajima, T. Tamegai, *Phys. Proc.* **27**, 104 (2012).

- ¹⁵ H. Lei, K. Wang, R. Hu, H. Ryu, M. Abeykoon, E. S. Bozin, and C. Petrovic, *Sci. Technol. Adv. Mater.* **13**, 054305 (2012)
- ¹⁶ E. J. Kramer, *J. Appl. Phys.* **44**, 1360 (1973).
- ¹⁷ D. Dew-Hughes, *Philos. Mag.* **30**, 293 (1974).
- ¹⁸ G. Antesberger, H. Ullmaier, *Philos. Mag.* **2-9**, 1101 (1974).
- ¹⁹ A. M. Campbell, J. E. Evetts, *Adv. Phys.* **21**, 199 (1972).
- ²⁰ W. A. Fietz, M. R. Beasley, J. Silcox, W. W. Webb, *Phys. Rev.* **136**, 335 (1964).
- ²¹ I. Adaktylos and H. W. Weber, *Phil. Mag.* **35**, 983 (1977).
- ²² R. Flükiger, C. Senatore, M. Cesaretti, F. Buta, D. Uglietti, and B. Seeber, *Supercond. Sci. Technol.* **21**, 054015 (2008).
- ²³ G. Blatter, M. V. Feigel'man, V. B. Geshkenbein, A. I. Larkin, and V. M. Vinokur, *Rev. Mod. Phys.* **66**, 1125 (1994).
- ²⁴ R. Ma, Y. Ma, W. Song, X. Zhu, S. Liu, J. Du, Y. Sun, C. Li, P. Ji, Y. Feng, P. Zhang, *Physica C* **411**, 77 (2004).
- ²⁵ P. Fabbriatore, C. Priano, A. Sciutti, G. Gemme, R. Musenich, R. Parodi, F. Gömöry, J.R. Thompson, *Phys. Rev. B* **54**, 12543 (1996).
- ²⁶ M. R. Koblishka, *Physica C* **282-287**, 2193 (1997), and references therein.
- ²⁷ M..R. Koblishka, A.J.J. van Dalen, T. Higuchi, S. I. Yoo, M. Murakami, *Phys. Rev. B* **58**, 2863 (1998).
- ²⁸ M. R. Koblishka, T. Higuchi, S.I. Yoo, M. Murakami, *J. Appl. Phys.* **85**, 3241 (1999).
- ²⁹ M. R. Koblishka, M. Muralidhar, M. Murakami, *Mater. Sci. Eng. B* **65**, 58 (1999).
- ³⁰ M. R. Koblishka, and M. Murakami, *Superconductors*, *Supercond. Sci. Technol.* **13**, 738 (2000).
- ³¹ M. R. Koblishka, *Tsinghua Science and Technology* **8**, 280 (2003).
- ³² M. R. Koblishka, *Inst. Phys. Conf. Ser.* **158**, 1141 (1997).
- ³³ M. R. Koblishka, M. Muralidhar, and M. Murakami, *Appl. Phys. Lett.* **73**, 2351 (1998).
- ³⁴ M. R. Koblishka, *phys. stat. sol. (a)* **189**, R1 (2002).
- ³⁵ M. R. Koblishka, M. Muralidhar, *Physica C* **496**, in print.
- ³⁶ M. R. Koblishka and J. Sosnowski, *Eur. Phys. J. B* **44**, 277 (2005).
- ³⁷ U. Welp, G. W. Crabtree, J. L. Wagner, and D. G. Hinks, *Physica C* **218**, 373 (1993).
- ³⁸ V. Sandu, *Mod. Phys. Lett. B* **26**, 1230007 (2012).
- ³⁹ H. Yang, H. Luo, Z. Wang, and H. H. Wen, *Appl. Phys. Lett.* **93**, 142506 (2008)

- ⁴⁰ A. Yamamoto, J. Jaroszynski, C. Tarantini, L. Balicas, J. Jiang, A. Gurevich, D. C. Larbalestier, R. Jin, A. S. Sefat, M. A. McGuire, B. C. Sales, D. K. Christen, and D. Mandrus, Appl. Phys. Lett. **94**, 062511 (2009)
- ⁴¹ D. L. Sun, Y. Liu, and C. T. Lin, Phys. Rev. B **80**, 144515 (2009)
- ⁴² L. Fang, Y. Jia, C. Chaparro, G. Sheet, H. Claus, M. A. Kirk, A. E. Koshelev, U. Welp, G. W. Crabtree, W. K. Kwok, S. Zhu, H. F. Hu, J. M. Zuo, H.-H. Wen, and B. Shen, Appl. Phys. Lett. **101**, 012601 (2012).
- ⁴³ C. Tarantini, S. Lee, Y. Zhang, J. Jiang, C. W. Bark, J. D. Weiss, A. Polyanskii, C. T. Nelson, H. W. Jang, C. M. Folkman, S. H. Baek, X. Q. Pan, A. Gurevich, E. E. Hellstrom, C. B. Eom, and D. C. Larbalestier, Appl. Phys. Lett. **96**, 142510 (2010).
- ⁴⁴ L. Fang, Y. Jia, J. A. Schlueter, A. Kayani, Z. L. Xiao, H. Claus, U. Welp, A. E. Koshelev, G. W. Crabtree, and W.-K. Kwok, Phys. Rev. B **84**, 140504(R) (2011).
- ⁴⁵ S. Salem-Sugui Jr., L. Ghivelder, A. D. Alvarenga, L. F. Cohen, Huiqian Luo, and Xingye Lu, Phys. Rev. B **84**, 052510 (2011).
- ⁴⁶ N. Haberkorn, B. Maierov, M. Jaime, I. Usov, M. Miura, G. F. Chen, W. Yu, and L. Civale, Phys. Rev. B **84**, 064533 (2011)
- ⁴⁷ T. Katase, H. Hiramatsu, V. Matias, C. Sheehan, Y. Ishimaru, T. Kamiya, K. Tanabe, and H. Hosono, Appl. Phys. Lett. **98**, 242510 (2011)
- ⁴⁸ S. Trommler, J. Hänisch, V. Matias, R. Hühne, E. Reich, K. Iida, S. Haindl, L. Schultz and B. Holzapfel, Supercond. Sci. Technol. **25**, 084019 (2012).
- ⁴⁹ M. Shahbazi, X. L. Wang, K. Y. Choi, and S. X. Dou, Appl. Phys. Lett. **103**, 032605 (2013)
- ⁵⁰ M. R. Koblishka *et al.*, unpublished.
- ⁵¹ K. S. Pervakov, V. A. Vlasenko, E. P. Khlybov, A. Zaleski, V. M. Pudalov, and Yu. F. Eltsev, Supercond. Sci. Technol. **26**, 015008 (2013).
- ⁵² S. Sharma, K. Vinod, C. S. Sundar, and A. Bharathi, Supercond. Sci. Technol. **26**, 015009 (2013).
- ⁵³ A. K. Pramanik, S. Aswartham, A. U. B. Wolter, S. Wurmehl, V. Kataev, and B. Büchner, J. Phys.: Condens. Matter **25**, 495701 (2013).
- ⁵⁴ D. Ahmad, I. Park, G. C. Kim, J. H. Lee, Z.-A. Ren, Y. C. Kim, Physica C **469**, 1052 (2009).
- ⁵⁵ D. Ahmad, T. K. Song, I. S. Park, G. C. Kim, Z.-A. Ren, and Y. C. Kim, Mod. Phys. Lett. B **25**, 1939 (2011).

- ⁵⁶ P. J. W. Moll, R. Puzniak, F. Balakirev, K. Rogacki, J. Karpinski, N.D. Zhigadlo and B. Batlogg, *Nature Mater.* **9**, 628 (2010).
- ⁵⁷ M. Kidszun, S. Haindl, T. Thersleff, J. Hänisch, A. Kauffmann, K. Iida, J. Freudenberger, L. Schultz, and B. Holzapfel, *Phys. Rev. Lett.* **106**, 137001 (2010).
- ⁵⁸ D. Bhoi, P. Mandal, P. Choudhury, S. Dash, A. Banerjee, *Physica C* **471**, 258 (2011).
- ⁵⁹ J. C. Zhuang, y. Sun, Y. Ding, F. F. Yuan, J. T. Liu, and Z. X. Shi, *Mod. Phys. Lett. B* **26**, 1250197 (2012).
- ⁶⁰ J. B. Anooja, P. M. Aswathy, N. Varghese, K. Vinod, A. Bharathi, and U. Syamaprasad, *J. Alloy Comp.* **566**, 43 (2013).
- ⁶¹ C. S. Yadav, and P. L. Paulose, *Solid State Commun.* **151**, 216 (2011).
- ⁶² H. Lei, and C. Petrovic, *Phys. Rev. B* **84**, 212502 (2011).
- ⁶³ M. Bonura, E. Giannini, R. Viennois, and C. Senatore, *Phys. Rev. B* **85**, 134532 (2012).
- ⁶⁴ M. Shahbazi, X. L. Wang, S. X. Dou, H. Fang, and C. T. Lin, *J. Appl. Phys.* **113**, 17E115 (2013).
- ⁶⁵ L. Shlyk, M. Bischoff, E. Rose, and R. Niewa, *J. Appl. Phys.* **112**, 053914 (2012).
- ⁶⁶ Y. Yin, M. Zech, T. L. Williams, X. Wang, G. Wu, X. H. Chen, and J. E. Hoffman, *Phys. Rev. Lett.* **102**, 097002 (2009).
- ⁶⁷ F. Massee, Y. Huang, R. Huisman, S. de Jong, J. Goedkoop, and M. Golden, *Phys. Rev. B* **79**, 220517 (2009).
- ⁶⁸ M. R. Koblishka, and U. Hartmann, *Europhys. Lett.* **89**, 47002 (2010).
- ⁶⁹ T. P. Ying, X. L. Chen, G. Wang, S. F. Jin, T. T. Zhou, X. F. Lai, H. Zhang, and W. Y. Wang, *Scientific Rep.* **2**, 426 (2012).

Figure captions:

FIG. 1. Pinning force scaling, $F_p/F_{p,\max}$ versus $h = H_a/H_{\text{irr}}$, for the 122-family – both pnictides and selenides. The open symbols are used for thin film (7, 10, 11) and IBAD tape (12, 14) data, the filled symbols denote single crystal data, and the one data set of a polycrystalline sample (16) is indicated by stars. The data set (13) is the only experiment of a 122-selenide material (indicated by a darker background), and is drawn using a solid black line. Except for the thin film/IBAD tape data, a tendency towards peak positions $h_0 > 0.33$ is evident from the curves presented.

FIG. 2. Pinning force scaling, $F_p/F_{p,\max}$ versus $h = H_a/H_{\text{irr}}$, for the 1111-family. The open symbols are used for the thin film data (3), polycrystalline materials and single crystals are indicated using full symbols. The peak position of the thin film data is the lowest of all; all other curves exhibit quite high but distinctly different h_0 -values, with (5) yielding the largest h_0 of all iron-based superconducting materials investigated so far.

FIG. 3. Pinning force scaling, $F_p/F_{p,\max}$ versus $h = H_a/H_{\text{irr}}$, for the 11-family. All investigated materials are single crystals in this case. Practically all published data fall together, and the resulting peak position, h_0 , is approx. 0.3. For comparison, the data set (13) of the 122-family, which is also a iron selenide, is added for comparison. Although the peak position is similar to the other 11-family data, the high-field side reveals a much stronger pinning contribution.

FIG. 4. Pinning force scaling, $F_p/F_{p,\max}$ versus $h = H_a/H_{\text{irr}}$, for the 111-family. For this material, only one data set is published in the literature. The dashed line indicates the scaling function when using the fit parameters as published by the original authors; the symbols give the pinning function after a complete reworking of the data. The relative high peak position persists after the necessary reworking.

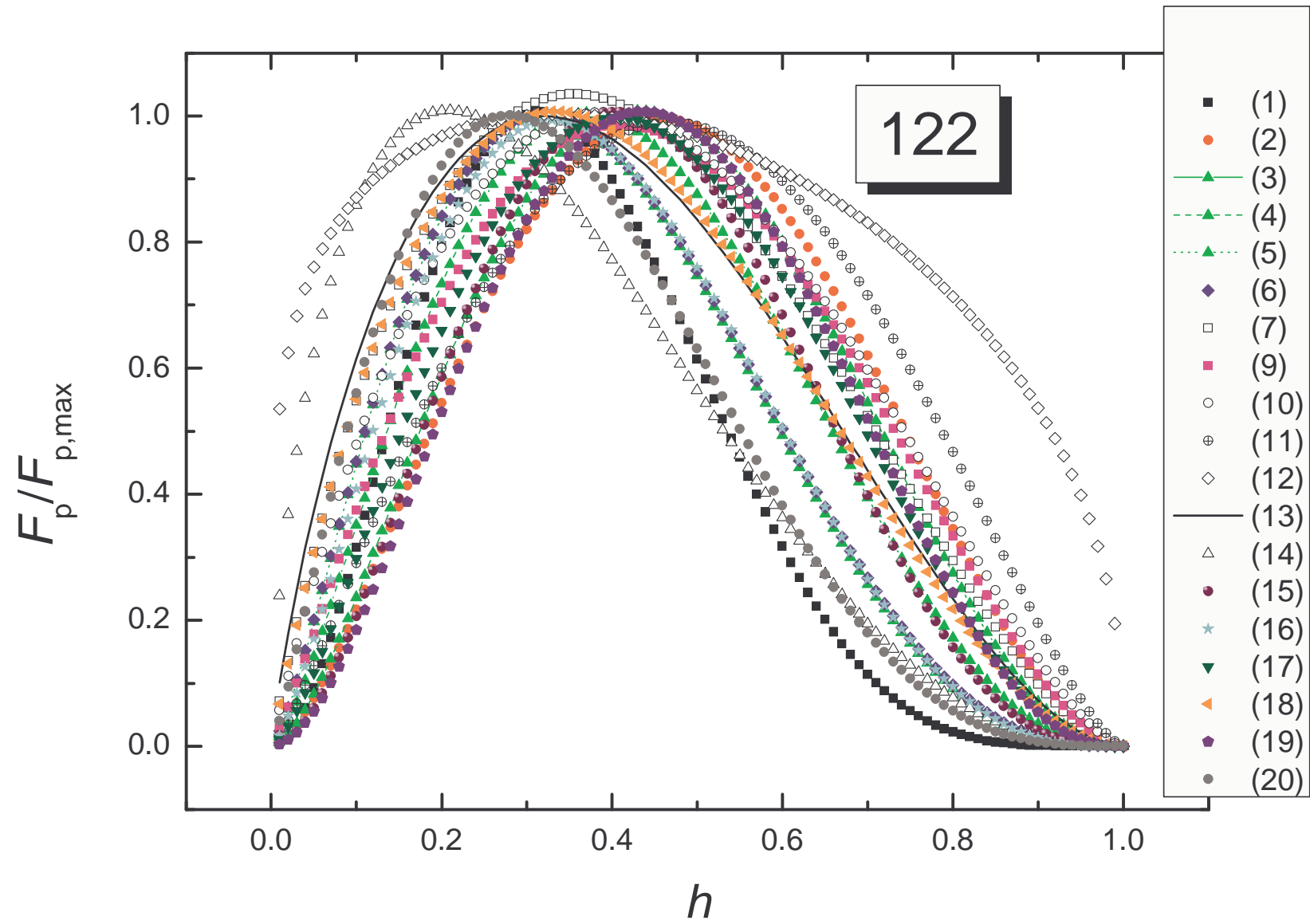


Fig.1

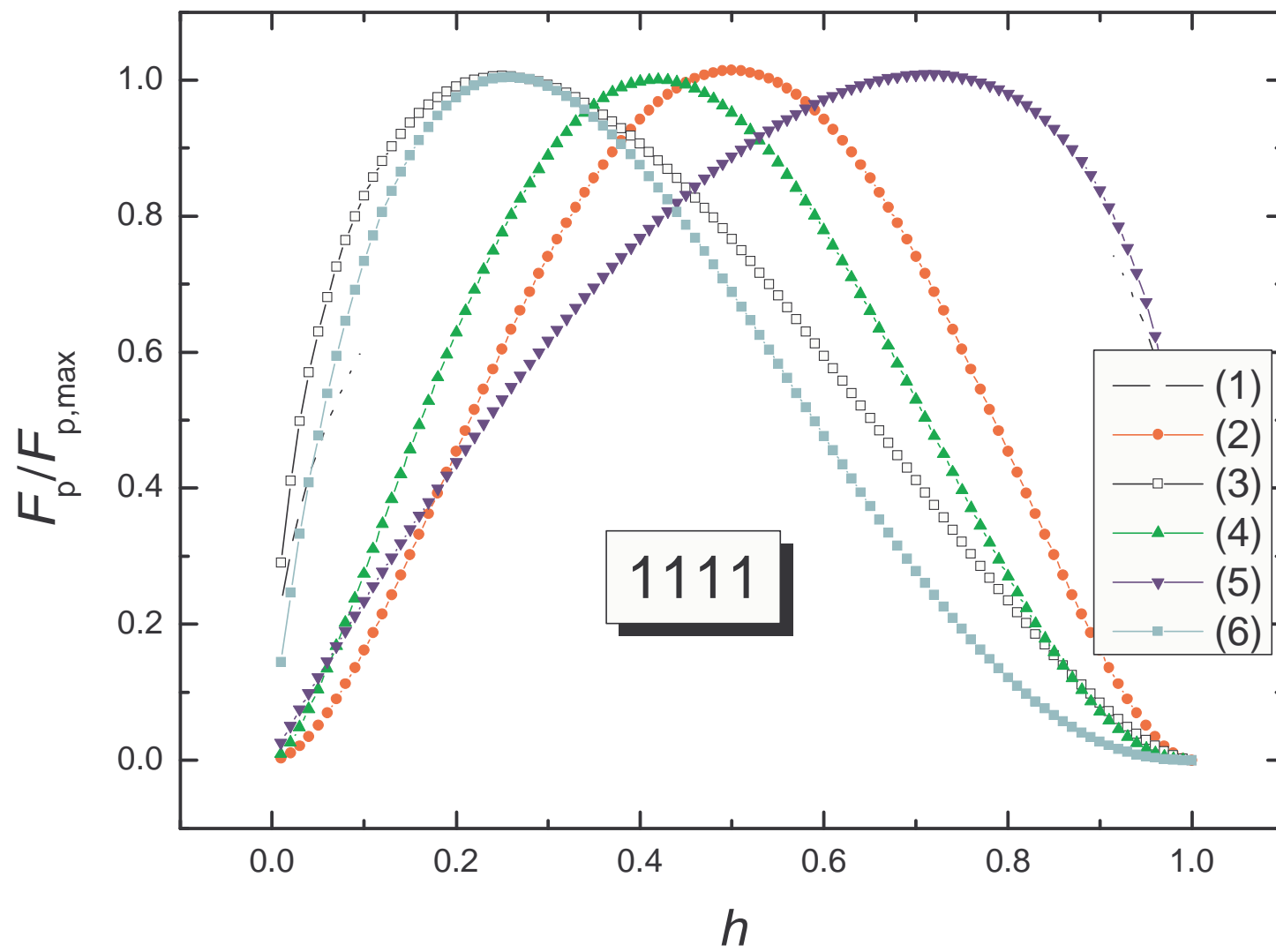


Fig.2

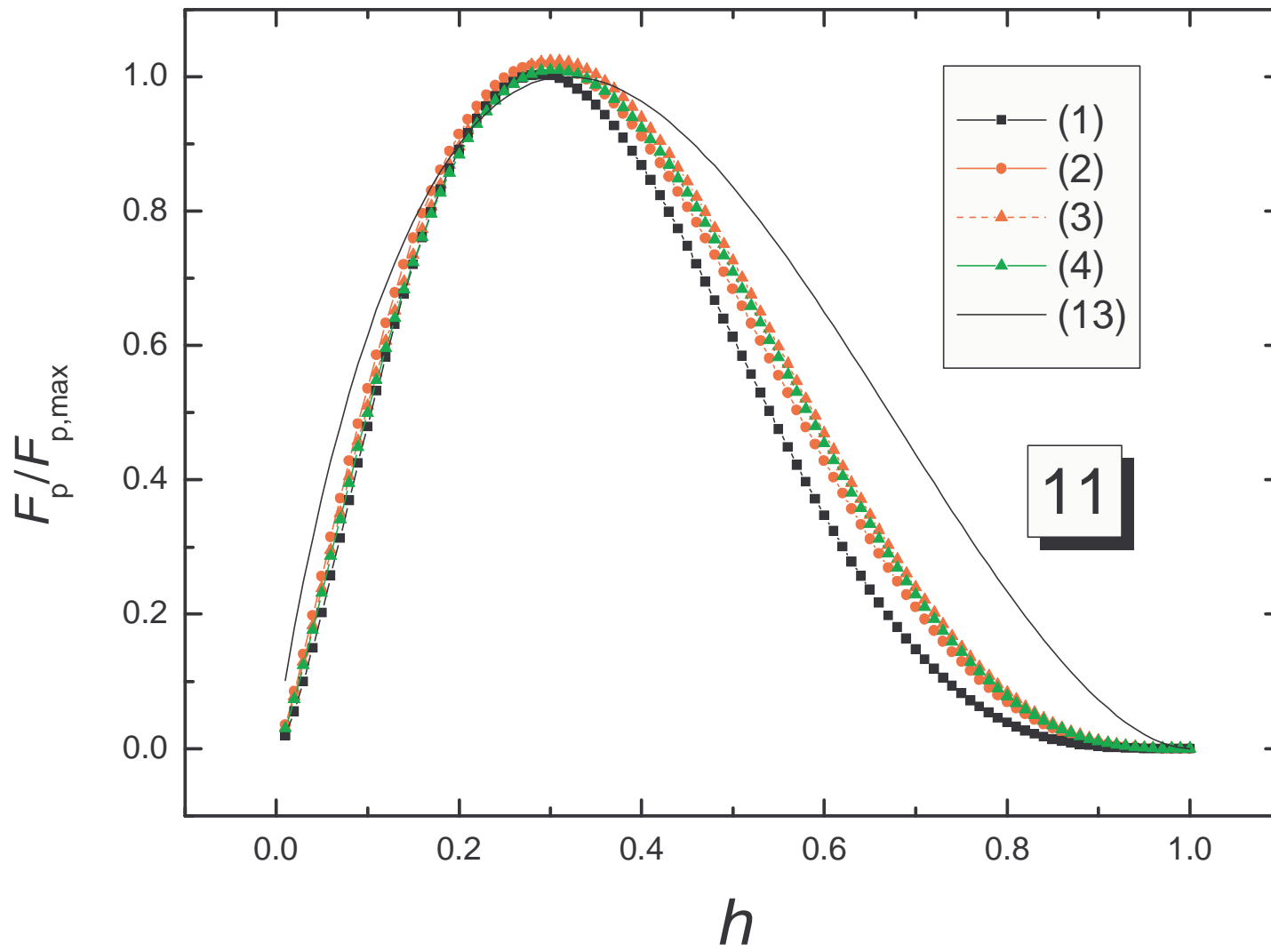


Fig.3

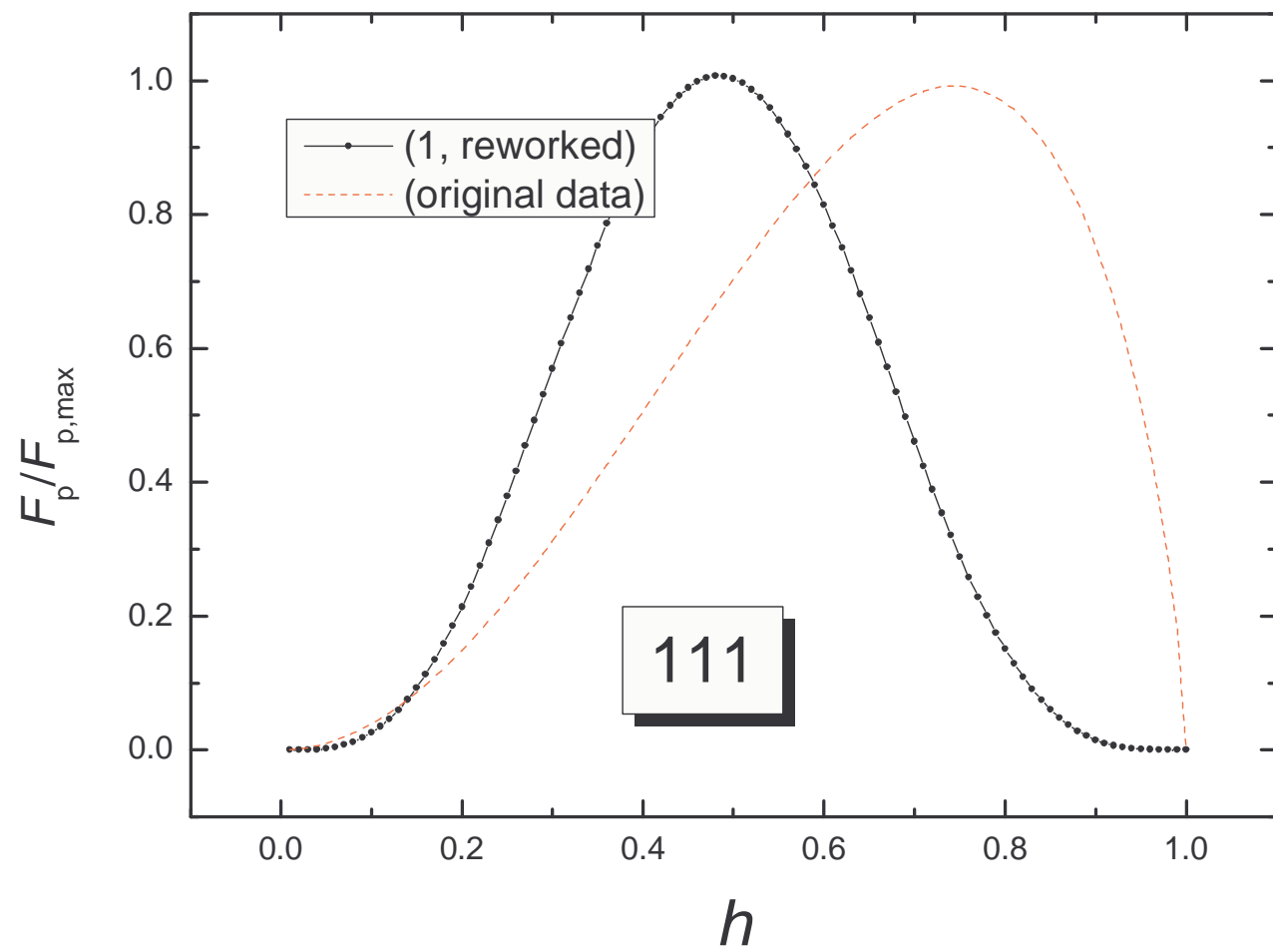


Fig.4